Zhang et al. Nanoscale Research Letters (2017) 12:412
DOI 10.1186/s11671-017-2180-z

Nanoscale Research Letters

NANO EXPRESS Open Access

$NiCo_2S_4$@$NiMoO_4$ Core-Shell Heterostructure Nanotube Arrays Grown on Ni Foam as a Binder-Free Electrode Displayed High Electrochemical Performance with High Capacity

Yan Zhang, Jie Xu*, Yayun Zheng, Yingjiu Zhang*, Xing Hu and Tingting Xu

Abstract

Core-shell-structured system has been proved as one of the best architecture for clean energy products owing to its inherited superiorities from both the core and the shell part, which can provide better conductivity and high surface area. Herein, a hierarchical core-shell $NiCo_2S_4$@$NiMoO_4$ heterostructure nanotube array on Ni foam (NF) ($NiCo_2S_4$@$NiMoO_4$/NF) has been successfully fabricated. Because of its novel heterostructure, the capacitive performance has been enhanced. A specific capacitance up to 2006 F g^{-1} was obtained at a current density of 5 mA cm^{-2}, which was far higher than that of pristine $NiCo_2S_4$ nanotube arrays (about 1264 F g^{-1}). More importantly, $NiCo_2S_4$@$NiMoO_4$/NF and active carbon (AC) were congregated as positive electrode and negative electrode in an asymmetric supercapacitor. As-fabricated $NiCo_2S_4$@$NiMoO_4$/NF//AC device has a good cyclic behavior with 78% capacitance retention over 2000 cycles, and exhibits a high energy density of 21.4 Wh kg^{-1} and power density of 58 W kg^{-1} at 2 mA cm^{-2}. As displayed, the $NiCo_2S_4$@$NiMoO_4$/NF core-shell herterostructure holds great promise for supercapacitors in energy storage.

Keywords: $NiCo_2S_4$@$NiMoO_4$, Core-shell, Nanotube arrays, Ni foam, Supercapaitor

Background

The ever increasing amount of energy consumption has motivated exploration of high-performance clean renewable energy [1–6]. Supercapacitors, considered as the promising dependable devices for energy storage, display excellent power density, rapid charge/discharge properties, long cycling stability, and environmental friendliness, which have received lots of attention from the researchers [7, 8]. At present, supercapacitors use high-surface-area carbon materials to store charge purely by electrostatic in nature (non-Faradaic electric double layers) [9], including carbon nanotube, graphene, and activated carbon. Capitalizing on Faradaic redox reactions, transition metal oxides, metal sulfides, or conducting polymers as pseudocapacitor electrode materials show higher specific capacitances than those carbonaceous electrode materials [2, 10]. Transition metal oxides have several advantages over other pseudocapacitive materials owning the properties of low toxicity, low cost, and natural abundance [11]. Among these transition metal oxides studied so far, ternary metal oxides, like $NiCo_2O_4$ [12], $CuCo_2O_4$ [13], $NiMoO_4$ [14], $CoMoO_4$ [15], and so on, can provide much higher electrical conductivity and richer electrochemical active sites than their single components, and they have been widely studied in the electrochemical energy field [12–15]. Although great progress has been made on ternary metal oxides electrodes to improve their electrochemical performance, these electrode materials still suffer from insufficient conductivity, slow ion diffusion rates, and serious volume change during the electrochemical procedure, which limit their further application for improving the performance of supercapacitors [16, 17]. Thus, it is vital to explore high-performance novel electrode materials

* Correspondence: xujie@zzu.edu.cn; zhangyj2006@zzu.edu.cn
School of Physical Engineering and Key Laboratory of Material Physics, Ministry of Education, Zhengzhou University, No. 75 Daxue Road, Zhengzhou 450052, China

to fulfill the increasing need for the electrochemical energy storage devices.

Lately, numerous attempts have been conducted to develop transition metal sulfides including CoS [18], NiS [19], CuS [20], Co_9S_8 [21], and $NiCo_2S_4$ [22] as supercapacitor electrode materials because of the gratifying electrical conductivity in comparison with the corresponding metal oxides [5]. Moreover, the ternary sulfides also can possess a higher conductivity and offer more richer redox reactions than those bare binary sulfides owing to the combine contributions from both metal ions [23, 24]. And $NiCo_2S_4$ as electrode has excellent electrochemical performance in energy devices [23–25]. However, many previous reports still demonstrate that most of the $NiCo_2S_4$ electrodes could not meet the requirement of high capacitance [26]. To address this issue, one possible solution is to design and synthesis different morphologies of metal sulfides with a large electrochemical active surface to enhance the electrochemical behavior. In particular, the core-shell heterostructure nanoarrays exhibit an efficient approach to improve the electrochemical behavior because it can provide many advantages such as the enlarged surface area, the increased conductivity and the synergistic effects produced by the core and shell materials [27].

Recently, various core-shell hybrid structure configurations have been fabricated such as $NiCo_2S_4$@$Ni(OH)_2$ [28], $NiCo_2S_4$@$Co(OH)_2$ [29], $NiCo_2O_4$@$NiMoO_4$ [30], Co_3O_4@$NiMoO_4$ [31], $NiMoO_4$@$Ni(OH)_2$ [32] and so forth, which have improved the electrochemical performance. Despite this progress, it is still a big challenge to fabricate the core-shell heterostructure with well-defined morphologies by effective and simple methods [33]. To further optimize the performance, the core-shell heterostructure can be directly grown on current collector which could offer good mechanical adhesion and electrical connection between the active materials and the substrates. Then, this configuration would increase the utilization of the active materials and lead to a higher capacitance [34].

Based on the above ideas, a core-shell heterostructure with the outer layer of $NiMoO_4$ nanosheets covering the $NiCo_2S_4$ nanotube arrays on Ni foam has been synthesized through a facile hydrothermal process and a heat treatment, which can be used as an advanced binder-free electrode. The as-prepared $NiCo_2S_4$@$NiMoO_4$/NF hybrid electrode exhibits a high specific capacitance up to 2006 F g^{-1} which is much higher than that of pristine $NiCo_2S_4$ nanotube arrays ($NiCo_2S_4$/NF) at 5 mA cm^{-2}, and a good cyclic performance of 75% capacitance retained over 2000 cycles at 50 mA cm^{-2}. Lately, an asymmetric supercapacitor based on $NiCo_2S_4$@$NiMo_2O_4$/NF and AC delivers a wide voltage window of 1.6 V, a maximum energy density of 21.4 Wh kg^{-1}, and a good cyclic stability of 78% capacitance retention at 40 mA cm^{-2} over 2000 cycles. The above results imply that the $NiCo_2S_4$@$NiMoO_4$/NF core-shell heterostructure is a promising electrode material in supercapacitor applications.

Methods

Synthesis of $NiCo_2S_4$/NF

The $NiCo_2S_4$/NF was fabricated through a two-step hydrothermal process similar to the previous reports [7, 26, 28]. Firstly, the Ni foam (1 × 4 cm) was cleaned in the HCl solution (3 mol L^{-1}) and acetone then washed thoroughly using deionized (DI) water and ethanol. The pre-treated Ni foam was obtained. Second, $Co(NO_3)_2 \cdot 6H_2O$, $Ni(NO_3)_2 \cdot 6H_2O$ and urea were dissolved in 70 mL DI water with a molar ration of 2:1:5. Then the system was moved in a Teflon-lined autoclave with the presence of cleaned Ni foam. After maintaining at 120 °C for 12 h, the Ni-Co precursor was successfully prepared. The $NiCo_2S_4$/NF was obtained by treating the Ni-Co precursor with Na_2S solution (0.03 mol L^{-1}) under the 90 °C for 12 h through an ion-exchange process. The average mass loading of as-prepared $NiCo_2S_4$/NF was around 2 mg cm^{-2}.

Synthesis of $NiCo_2S_4$@$NiMoO_4$/NF

The $NiCo_2S_4$@$NiMoO_4$/NF was prepared by a hydrothermal route combining with a calcination process were according to previously published works with some modified [32, 35]. Typically, the $NiCo_2S_4$/NF was put into the 70 mL solution containing 1 mmol $Ni(NO_3)_2 \cdot 6H_2O$ and 1 mmol $Na_2MoO_4 \cdot 2H_2O$ through a hydrothermal treatment under 100 °C for 4 h. Therein, the as-obtained sample was annealed by keeping the temperature at 400 °C for 2 h under Ar atmosphere. The mass loading of $NiCo_2S_4$@$NiMoO_4$ was about 3 mg cm^{-2}.

Material Characterization

The structure of the prepared materials was investigated using X-ray diffraction (XRD, Netherlands Philip X' Pert). The information of morphologies from the $NiCo_2S_4$/NF and $NiCo_2S_4$@$NiMoO_4$/NF was studied by scanning electron microscope (SEM, JSM-6700F, JEOL) and transmission electron microscope (TEM, JEM-2100, 200 kV, JEOL). X-ray photo-electron spectroscopy (XPS) measurements were conducted on Thermo Scientific ESCALAB 250XI spectrometer.

Electrochemical measurements

The three-electrode configuration was conducted on the electrochemical workstation (CS 2350, Wuhan) to analyze the electrochemical properties in 2 mol L^{-1} KOH electrolyte. The working electrode was $NiCo_2S_4$/NF and $NiCo_2S_4$@$NiMoO_4$/NF (1× 1 cm in area), the Pt foil was employed as the counter electrode and standard calomel electrode (SCE) was acted as the reference

electrode. Techniques contained cyclic voltammetry (CV), galvanostatic charge-discharge (GCD) and electrochemical impedance spectroscopy (EIS). The EIS tests were conducted with the frequency of 0.01 Hz~100 kHz and a superimposed sinusoidal voltage of 5 mV amplitude. Based on the discharge curves, the specific capacitances (C_s, F g^{-1}) were calculated on the basis of the following equation: $C_s = I\Delta t/m\Delta V$, where m (g), I (A), ΔV (V) and Δt (s) represent the mass, current, voltage window, and the time during the discharge procedure, respectively.

Fabrication of the Asymmetric Supercapacitor

Electrochemical measurements of the asymmetric supercapacitor (ASC) device were investigated in a two-electrode configuration. The configuration took $NiCo_2S_4$@$NiMoO_4$/NF and AC as the positive and negative electrode, respectively, a filter paper as separator. Then, we wrapped them with the tape for packaging. Afterwards, we immersed them in the electrolyte of 2 mol L^{-1} KOH and obtained the final assembled asymmetric $NiCo_2S_4$@$NiMoO_4$//AC device (Additional file 1: Figure S1). Particularly, the active carbon was mixed with 10 wt% acetylene black and 5 wt% polyvinylidene fluoride (PVDF) to form the slurry to prepare the AC electrode. Subsequently, the slurry was directly coated onto the pre-treated Ni foam (1 × 1 cm in area) and dried in vacuum at 60 °C for 12 h. The mass of the positive and negative electrodes were determined with the balance theory of $Q_+ = Q_-$ ($Q = C_s m\Delta V$) to ensure an efficient charge storage, where C_s (F g^{-1}), m (g) and ΔV (V) stand for the specific capacitance, mass of the electrode and the potential window, respectively. Based on the above balance theory, the optimal mass loading of the negative electrode of AC is about 24.84 mg cm^{-2}.

Results and Discussion

The fabrication process of the hierarchical $NiCo_2S_4$@$NiMoO_4$/NF is displayed in Fig. 1. Initially, under a two-step hydrothermal method which contains an in situ growth procedure and an ion-exchange process, the $NiCo_2S_4$ nanotube arrays on highly conductive microporous Ni foam were obtained. Subsequently, $NiMoO_4$ interconnected nanosheets shell was deposited on the backbone of $NiCo_2S_4$ nanotube arrays through a hydrothermal treatment as well as an annealing process.

The XRD pattern of as-prepared $NiCo_2S_4$@$NiMoO_4$ core-shell nanotube arrays on Ni foam is shown in Fig. 2. The substrate of Ni foam corresponds to three main peaks in the pattern. Several other strong peaks of 31.7°, 38.2°, 50.4°, and 55.5° can be well indexed to $NiCo_2S_4$ (PDF cards No. 43-1477), and the diffraction peaks of 31.4°, 36.9°, and 55.1° belong to $NiMoO_4$ (PDF cards No. 86-0362), which indicate the formation of the $NiCo_2S_4$ and $NiMoO_4$. Besides, the XPS

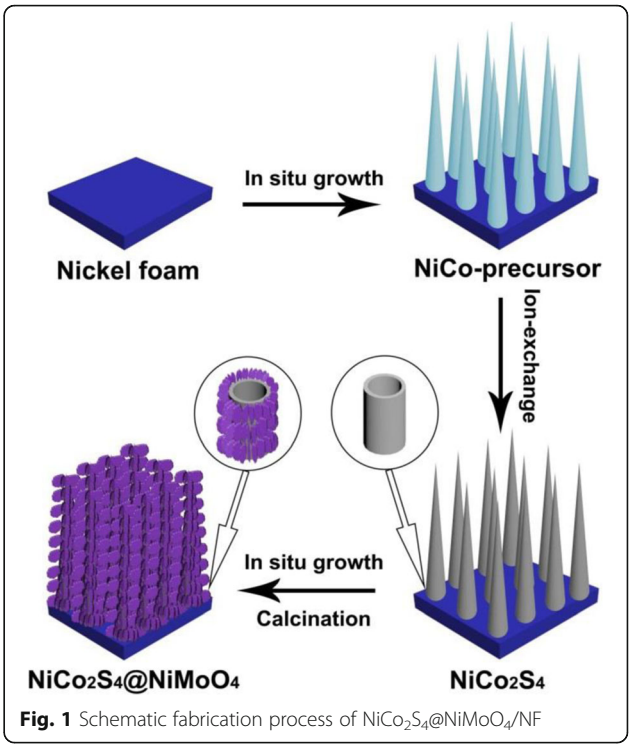

Fig. 1 Schematic fabrication process of $NiCo_2S_4$@$NiMoO_4$/NF

results of the as-prepared $NiCo_2S_4$@$NiMoO_4$ are shown in Additional file 1: Figure S2. The full survey spectrum mainly displays that presence of the Ni 2p, Co 2p, Mo 3d, S 2p, O 1 s in the product (Additional file 1: Figure S2A). The binding energies of Ni 2p and Co 2p are in accordance with the formation of $NiCo_2S_4$ [36, 37]. The XPS results as shown in Additional file 1: Figure S2 display that the composite contains Ni^{2+}, Ni^{3+}, Co^{2+}, Co^{3+} and Mo^{6+}, which are agree with the phase structure of $NiCo_2S_4$@$NiMoO_4$ [36, 38, 39].

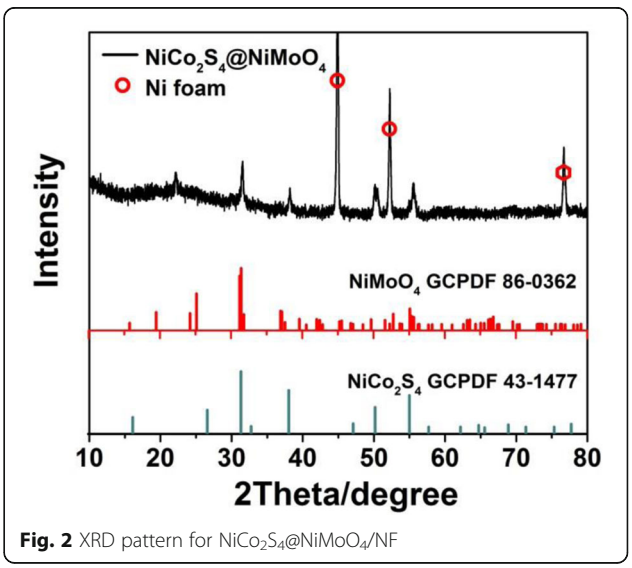

Fig. 2 XRD pattern for $NiCo_2S_4$@$NiMoO_4$/NF

The general morphologies and microstructure of the $NiCo_2S_4$/NF and $NiCo_2S_4$@$NiMoO_4$/NF electrode materials are presented in Fig. 3. The SEM images at different magnifications of the $NiCo_2S_4$ nanotubes on Ni foam are displayed in Fig. 3a–c. From the images in Fig. 3a and b, a grass-like three-dimensional (3D) nanostructure homogeneously covered on the substrate of Ni foam was formed by a large number of $NiCo_2S_4$ nanotubes. And, the diameter of the nanotube is approximately 70–100 nm (Fig. 3c). Afterward, the surface of $NiCo_2S_4$ nanotubes turns rough, and a layer shell of $NiMoO_4$ interconnecting nanosheets is fully deposited on the surface of $NiCo_2S_4$ nanotubes, which results in a hierarchical core-shell heterostructure (as shown in Fig. 3d–f). The obtained $NiCo_2S_4$@$NiMoO_4$ nanotubes are well aligned on Ni foam skeletons in large-scale (Fig. 3d and inset). The higher magnification SEM images (Fig. 3e and f) reveal that the $NiMoO_4$ nanosheets are crossed-linked with each other and filling both the surface of the $NiCo_2S_4$ nanotubes and the spaces between them. Therefore, a high specific-surface-area construction has been generated and the $NiCo_2S_4$@$NiMoO_4$ nanotubes have an average diameter around 700 nm. The detailed structure of $NiCo_2S_4$/NF and $NiCo_2S_4$@$NiMoO_4$/NF is further provided by TEM. Figure 3g exhibits the TEM images of $NiCo_2S_4$ nanotubes scraped from Ni foam. The image shows that the $NiCo_2S_4$ nanotubes have a clear hollow nanostructure. The magnified image inset in Fig. 3g at lower left shows that the $NiCo_2S_4$ nanotube displays the shell thickness of 15 ± 2 nm. The inset at the upper right further confirmed the formation of $NiCo_2S_4$ with a lattice spacing of 0.28 nm in according with the (311) plane of cubic phase. The TEM images (Fig. 3h) of $NiCo_2S_4$@$NiMoO_4$/NF confirm that the $NiMoO_4$ nanosheets are uniformly covered on the surface of $NiCo_2S_4$ nanotubes, and the thickness of $NiMoO_4$ shell is around 300 nm which is consistent with the SEM images. Figure 3h inset clearly exhibits the layer containing a large number of thin nanosheets full of stack and folds which is benefit to the ion diffusion during the electrochemical reaction. HRTEM (High Resolution Transmission Electron Microscopy) image shows the lattice fringes of 0.243 nm are matched well with the (021) plane of the $NiMoO_4$ layer (Fig. 3i). The above results demonstrate the $NiCo_2S_4$@$NiMoO_4$ core-shell nanotubes have been built which is in accordance with the XRD patterns.

The electrochemical performance of $NiCo_2S_4$/NF and $NiCo_2S_4$@$NiMoO_4$/NF binder-free electrodes were studied in a three-electrode configuration by measuring techniques of CV, GCD and EIS (Fig. 4, Additional file 1: Figure S3 and S4). Figure 4a exhibits the CV curves of $NiCo_2S_4$/NF electrode and $NiCo_2S_4$@$NiMoO_4$/NF electrode with a potential window of 0–0.5 V at 10 mV s^{-1}. For the $NiCo_2S_4$/NF electrode, a couple of redox peaks

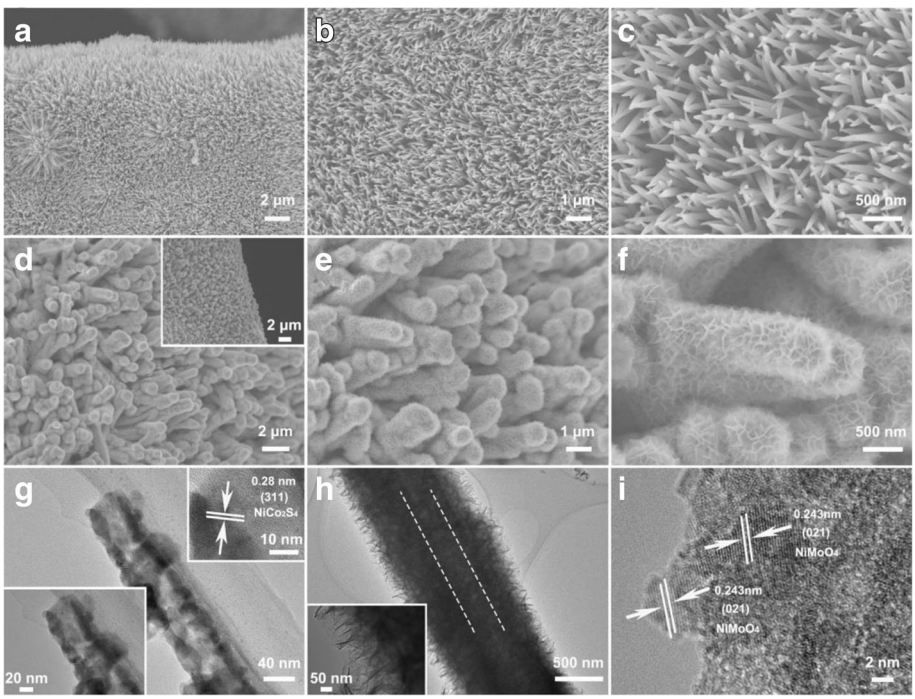

Fig. 3 SEM images for $NiCo_2S_4$/NF (**a**–**c**) and $NiCo_2S_4$@$NiMoO_4$/NF (**d**–**f**) at different magnifications. **g** TEM images of an individual $NiCo_2S_4$ nanotube detached from Ni foam; the above *inset* is the corresponding HRTEM image of a single nanotube. **h** TEM images and **i** HRTEM images of an individual $NiCo_2S_4$@$NiMoO_4$ core-shell structure

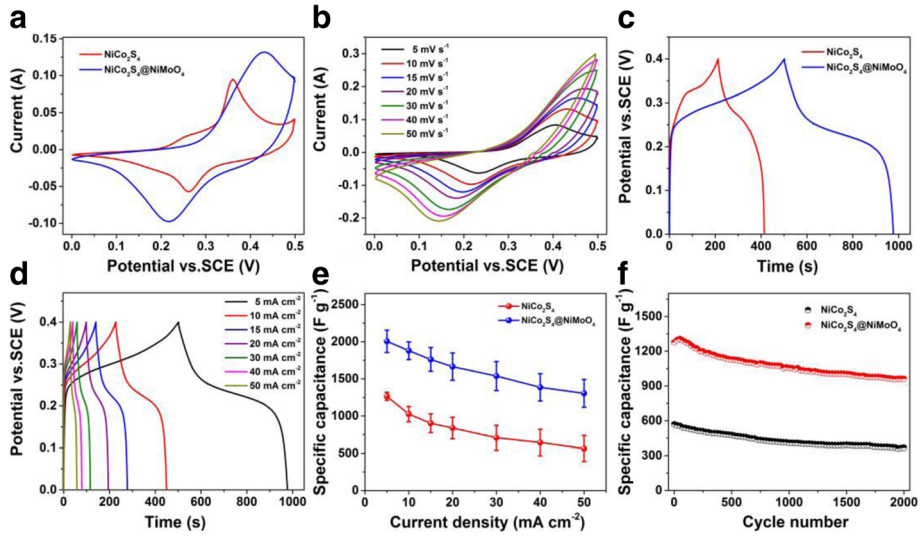

Fig. 4 **a** The comparison of the CV curves of $NiCo_2S_4$, $NiCo_2S_4$@$NiMoO_4$ at the scan rate of 10 mV s^{-2}. **b** CV curves of the $NiCo_2S_4$@$NiMoO_4$ product at the scan rates of 5, 10, 15, 20, 30, 40, 50 mV s^{-1}. **c** Comparison of GCD curves of the $NiCo_2S_4$, $NiCo_2S_4$@$NiMoO_4$ at a current density of 5 mA cm^{-2}. **d** GCD curves of the $NiCo_2S_4$@$NiMoO_4$ composite at the current densities of 5, 10, 15, 20, 30, 40, 50 mA cm^{-2}. **e** Specific capacitance of the $NiCo_2S_4$, $NiCo_2S_4$@$NiMoO_4$ composite at different current densities. **f** Cycling performance of $NiCo_2S_4$, $NiCo_2S_4$@$NiMoO_4$ composite at 50 mA cm^{-2} for 2000 cycles

are visible, which are mainly coming from the redox reactions in regard to the M^{2+}/M^{3+} (M = Ni, Co) redox couples [28], demonstrating the typical pseudocapacitive performance. For the $NiCo_2S_4$@$NiMoO_4$/NF electrode, the expanded peaks are due to the M^{2+}/M^{3+} (M = Ni, Co) redox couples from the $NiCo_2S_4$ core and the Ni^{2+}/Ni^{3+} redox couples of the $NiMoO_4$ shell. During the electrochemical process, the redox reaction of Mo atom does not occur. Then, the redox behavior of Mo has no contribution to the tested capacitance [32]. The Mo element played a key role is to improve the conductivity of the ternary metal oxides and to gain the enhanced electrochemical performance [6]. The capacitances of the electrode are represented by the areas surrounded by the CV curves. Compared with the $NiCo_2S_4$/NF, the $NiCo_2S_4$@$NiMoO_4$/NF electrode owned an enlarged area by the presence of $NiMoO_4$ nanosheets, revealing the hybrid core-shell electrode possesses a higher specific capacitance. The CV curves of $NiCo_2S_4$@$NiMoO_4$/NF and $NiCo_2S_4$/NF electrode at various scan rates are showed in Fig. 4b and Additional file 1: Figure S3A, respectively. The shapes of the curves and the presence of the redox peaks both demonstrate the pseudocapacitive nature of the electrode. As the scan rate increased, the shape of all the curves is still maintained with a little shift of the peaks position owing to the polarization behavior of the electrodes [35]. The GCD measurement determines the capacitive property of $NiCo_2S_4$/NF electrode and $NiCo_2S_4$@$NiMoO_4$/NF hybrid electrode. Compared with the pristine $NiCo_2S_4$, the $NiCo_2S_4$@$NiMoO_4$ could store more charges due to it delivers a longer discharging time at 5 mA cm^{-2} (Fig. 4c). Besides, in each curve, there is a distinct voltage plateau existing in the charge/discharge process, which reveals the capacitance characteristics generating from the redox reactions, which is consistent with the CV curves. Figure 4d and Additional file 1: Figure S3B display the GCD curves of the prepared electrodes at different current densities. There is a distinct plateau region in every curve proving the pseudocapacitive performance of electrodes. Figure 4e shows the specific capacitances at various current densities of the prepared two electrodes. The specific capacitance of the bare $NiCo_2S_4$ was calculated to be 1264, 1025, 903, 838, 708, 645, 572 F g^{-1} at 5, 10, 15, 20, 30, 40, 50 mA cm^{-2}, respectively. In contrast with the bare $NiCo_2S_4$, the $NiCo_2S_4$@$NiMoO_4$ displays the significantly enhanced specific capacitances as high as 2006, 1879, 1761, 1664, 1538, 1386, 1305 F g^{-1} at the current densities of 5, 10, 15, 20, 30, 40, 50 mA cm^{-2}, respectively. The hybrid electrode possesses a higher capacity mainly due to the five merits as follows: (1) The designed core-shell hybrid configuration and the microporous feature for 3D Ni foam facilitate the diffusion of the electrolyte ions. (2) For redox reactions, the nanotube arrays could result in more exposed electroactive sites. (3) The porous $NiCo_2S_4$ skeleton with high conductivity builds the electrical conductive pathways for active materials leading to the enhanced conductivity and a fast reversible redox reaction. (4) The binder-free characteristic of the $NiCo_2S_4$@$NiMoO_4$ enables a low interfacial resistance and the absence of addictive would greatly reduce the "inactive" surface in the electrode [26, 40]. (5) The synergistic effect of the $NiCo_2S_4$

nanotubes core and $NiMoO_4$ nanosheets shell also provides a positive effect on the capacitance. Based on the calculated capacitive results showed in Fig. 4e, the capacitance of $NiCo_2S_4$@$NiMoO_4$ remains around 65.1% with the increasing of current density, which is higher than the pristine $NiCo_2S_4$ (45.3%). Therefore, the good rate capability is not only owing to the higher conductivity of the $NiCo_2S_4$, but also due to the highly porous structure of the interconnected $NiMoO_4$ nanosheets filled both on the surface of the $NiCo_2S_4$ nanotubes as well as the spaces between them, which further increases the accessibility of the microscopic area.

The cyclic performance plays an important role in supercapacitor devices. Figure 4f shows the cycling stabilities of the $NiCo_2S_4$ and $NiCo_2S_4$@$NiMoO_4$ hybrid electrodes after 2000 cycles at 50 mA cm^{-2}. With the cycle number increasing, the specific capacitance gradually decreases. Over 2000 cycles, there is still 75.3% of its initial capacitance retained and it performs better than $NiCo_2S_4$ (64.6% over 2000 cycles). For $NiCo_2S_4$@$NiMoO_4$ electrode, the specific capacitance increases at the initial 100 cycles, which is because the electrode activation increases the available active sites [41]. Besides, EIS measurement was carried out to further examine the excellent electrochemical performance of the $NiCo_2S_4$@$NiMoO_4$ electrode. Additional file 1: Figure S4 displays the impedance Nyquist plots of the $NiCo_2S_4$@$NiMoO_4$ hybrid electrode before and after 2000 cycles. The Nyquist plots were similar to each other which contained a quasi-semicircle in the high frequency region and a straight line in the low frequency region. The straight line in the low frequency region shows the Warburg resistance which is ascribed to the diffusion behavior of the electrolyte to the electrode surface [42, 43]. And the Warburg resistances of the

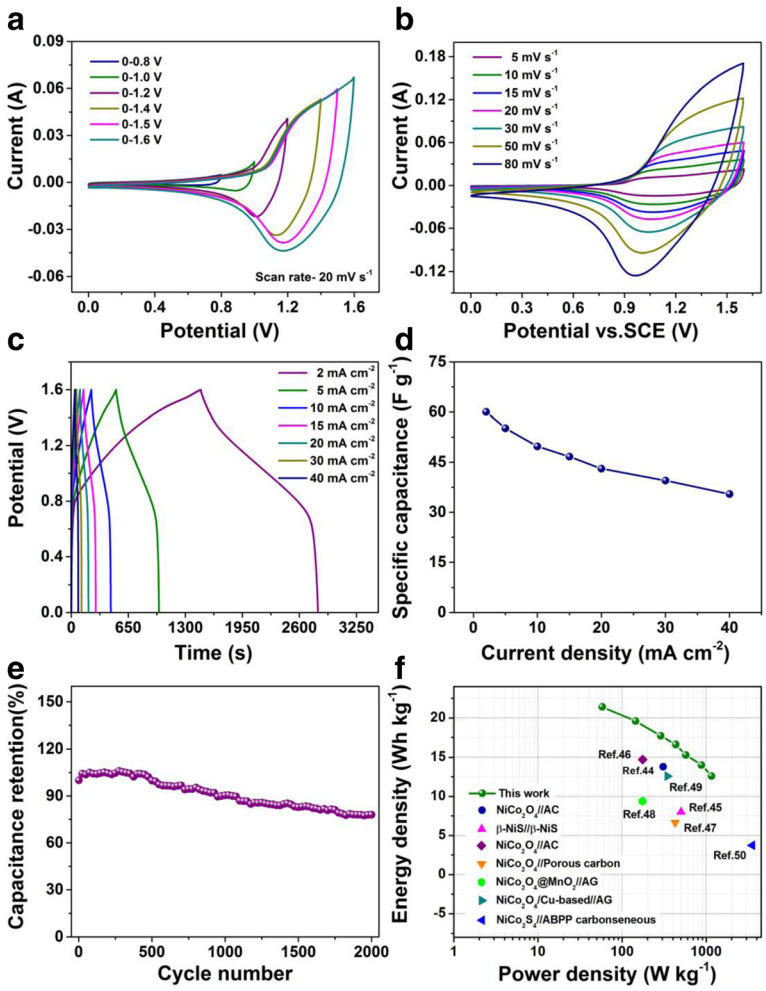

Fig. 5 **a** CV curves of $NiCo_2S_4$@$NiMoO_4$//AC asymmetric supercapacitor collected in different voltage windows at 20 mV s^{-1}. **b** CV curves of $NiCo_2S_4$@$NiMoO_4$//AC at different scan rates. **c** GCD curves of $NiCo_2S_4$@$NiMoO_4$//AC at different current densities. **d** Specific capacitances of $NiCo_2S_4$@$NiMoO_4$//AC at different current densities. **e** Cycling performance of $NiCo_2S_4$@$NiMoO_4$//AC at 40 mA cm^{-2}. **f** Ragone plots of energy density and power density of $NiCo_2S_4$@$NiMoO_4$//AC

hybrid electrode before and after cycling are almost unchanged, indicating the good cyclic stability of this electrode. And this is in accordance with the electrochemical performance analyzed above.

To value the potential application of $NiCo_2S_4$@$NiMoO_4$ electrode in supercapacitors, an asymmetric supercapacitor device in a two-electrode configuration was constructed with the $NiCo_2S_4$@$NiMoO_4$ and AC electrode act as the positive electrode and negative electrode with the area of 1 cm^2, respectively, a filter paper as the separator and 2 mol L^{-1} KOH as the electrolyte. The specific capacitance of active carbon is 85.07 F g^{-1} at a current density of 5 A g^{-1} (Additional file 1: Figure S5). Figure 5a shows the CV curves of the device at various voltage windows from 0–0.8 to 0–1.6 V. From the image we obtained the voltage window of the ASC device can achieve 1.6 V as expected. The CV curves of the device at different scan rates are shown in Fig. 5b. The shapes of the CV curves at various scan rates are almost maintained, revealing the excellent capacitance behavior of the ASC device. GCD curves of the $NiCo_2S_4$@$NiMoO_4$//AC device from 2 to 40 mA cm^{-2} in the potential window of 0–1.6 V are further illustrated in Fig. 5c. The specific capacitance evaluated from the discharging curves are 60.05, 55.16, 49.74, 46.66, 43.06, 39.50, and 35.45 F g^{-1} at 2, 5,10, 15, 20, 30, and 40 mA cm^{-2}, respectively, as exhibited in Fig. 5d. The cycling life of the capacitor has been measured by the virtue of GCD cycling at 40 mA cm^{-2} (Fig. 5e). After 2000 cycles, the specific capacitance remains 78%, demonstrating its good cycle stability. The Impedance Nyquist plots of the $NiCo_2S_4$@$NiMoO_4$//AC device before and after 2000 cycles have been shown in Additional file 1: Figure S6. The plots show that the Warburg resistances of the device are almost have no change before and after cycling, demonstrating the good stability of the asymmetric device. Figure 5f displays the relations between the energy density and power density in contrast with other devices. The $NiCo_2S_4$@$NiMoO_4$//AC device displays 21.4 Wh kg^{-1} at 58 W kg^{-1}, and still maintains 12.6 Wh kg^{-1} at a power density of 1158 W kg^{-1}. As compared to previous reported publications, the energy density of our work is higher than those of $NiCo_2O_4$//AC (13.8 Wh kg^{-1}) [44], β-NiS//β-NiS (7.97 Wh kg^{-1}) [45], $NiCo_2O_4$//AC (14.7 Wh kg^{-1}) [46], $NiCo_2O_4$// Porous carbon (6.61 Wh kg^{-1}) [47], $NiCo_2O_4$@MnO_2//AG (activated graphenes) (9.4 Wh kg^{-1}) [48], $NiCo_2O_4$/Cu-based//AG (12.6 Wh kg^{-1}) [49], $NiCo_2S_4$//ABPP (activated balsam pear pulp) carbonceneous (3.72 Wh kg^{-1}) [50].

Conclusions

In short, novel hierarchical $NiCo_2S_4$@$NiMoO_4$ nanotube arrays with the core-shell heterostructure have been successfully deposited on Ni foam. As the electrode for supercapacitors, it displays a high specific capacitance of 2006 F g^{-1} at 5 mA cm^{-2} and a good cyclic stability (75% after 2000 cycles at 50 mA cm^{-2}). Moreover, an asymmetric supercapacitor has been obtained based on $NiCo_2S_4$@$NiMoO_4$ and AC as the positive and negative electrode, respectively, which achieves a specific capacitance of 60.05 F g^{-1} at 2 mA cm^{-2} with a potential window of 1.6 V. It also delivers a maximum energy density of 21.4 Wh kg^{-1} and a good cyclic stability (78% over 2000 cycles at 40 mA cm^{-2}), which make it a promising candidate in the field of supercapacitors.

Additional file

Additional file 1: Supporting information. **Figure S1.** Schematic illustration (A) and photograph (B) of the as-fabricated $NiCo_2S_4$@$NiMoO_4$// AC device. **Figure S2.** XPS spectra of the (A) survey spectrum, (B) Ni 2p, (C) Co 2p, (D) Mo 3d, (E) S 2p and (F) O 1 s of the $NiCo_2S_4$@$NiMoO_4$ composite. **Figure S3.** (A) CV curves at different scan rates and (B) GCD curves at different current densities of $NiCo_2S_4$. **Figure S4.** Impedance Nyquist plots of the $NiCo_2S_4$@$NiMoO_4$ hybrid electrode before and after 2000 cycles in a three-electrode system. **Figure S5.** CV curves of the AC electrode at different scan rates (A), GCD curves of the AC electrode at different current densities (B), the specific capacitance change of the AC electrode at different current densities (C). **Figure S6.** Impedance Nyquist plots of the $NiCo_2S_4$@$NiMoO_4$//AC device before and after 2000 cycles. (DOCX 2512 kb)

Abbreviations

ABPP: Activated balsam pear pulp; AC: Active carbon; AG: Activated graphenes; ASC: Asymmetric supercapacitor; CV: Cyclic voltammetry; DI: Deionized; EIS: Electrochemical impedance spectroscopy; GCD: Galvanostatic charge-discharge; HRTEM: High-resolution transmission electron microscopy; NF: Ni foam; PVDF: Polyvinylidene fluoride; SCE: Standard calomel electrode; SEM: Scanning electron microscope; TEM: Transmission electron microscope; XPS: X-ray photo-electron spectroscopy; XRD: X-ray diffraction

Acknowledgements

The present work is financially supported by the Natural Science Foundation under the grants of NSFC (51602289), the Startup Research Fund of Zhengzhou University (51090104), and the Outstanding Young Talent Research Fund of Zhengzhou University (32210461).

Authors' Contributions

ZY carried out the experiment and data analysis and finalized manuscript. XJ provided the experimental program, participated in data analysis, and manuscript-revising work. ZYY contributed to the modification of the article. ZYJ, HX, and XTT provided helpful proposal for the experiment. All authors read and approved the final manuscript.

Competing Interests

The authors declare that they have no competing interests.

Publisher's Note

Received: 21 February 2017 Accepted: 1 June 2017
Published online: 15 June 2017

References

1. Kong SY, Cheng K, Gao YY, Ouyang T, Ye K, Wang GL et al (2016) A novel three-dimensional manganese dioxide electrode for high performance supercapacitors. J Power Sources 308:141–148
2. Ajay A, Paravannoor A, Joseph J, Amruthalakshmi V, Anoop SS, Nair SV et al (2015) 2D amorphous frameworks of $NiMoO_4$ for supercapacitors: defining

the role of surface and bulk controlled diffusion processes. Appl Surf Sci 326:39–47
3. Wang JG, Jin DD, Zhou R, Shen C, Xie KY, Wei BQ (2016) One-step synthesis of $NiCo_2S_4$ ultrathin nanosheets on conductive substrates as advanced electrodes for high-efficient energy storage. J Power Sources 306:100–106
4. Cai PD, Liu B, Wang DD, Wang LL, Liu Y, Li H et al (2014) Construction of unique $NiCo_2O_4$ nanowire@$CoMoO_4$ nanoplate core/shell arrays on Ni foam for high areal capacitance supercapacitors. J Mater Chem A 2:4954–4960
5. Ghosh D, Das CK (2015) Hydrothermal growth of hierarchical Ni_3S_2 and Co_3S_4 on a reduced graphene oxide hydrogel@Ni foam: a high-energy-density aqueous asymmetric supercapacitor. ACS Appl Mater Interfaces 7: 1122–1131
6. Cai DP, Liu B, Wang DD, Liu Y, Wang LL, Han L, Wang YR, Wang CX, Li QH, Wang TH (2014) Enhanced performance of supercapacitors with ultrathin mesoporous $NiMoO_4$ nanosheets. Electrochim Acta 125:294–301
7. Chen HC, Jiang JJ, Zhang L, Xia DD, Zhao YD, Guo DQ et al (2014) In situ growth of $NiCo_2S_4$ nanotube arrays on Ni foam for supercapacitors: maximizing utilization efficiency at high mass loading to achieve ultrahigh areal pseudocapacitance. J Power Sources 254:249–257
8. Ma LB, Shen XP, Zhou H, Ji ZY, Chen KM, Zhu GX (2015) High performance supercapacitor electrode materials based on porous $NiCo_2O_4$ hexagonal nanoplates/reduced graphene oxide composites. Chem Eng J 262:980–988
9. Ray RS, Sarma B, Jurovitzki AL, Misra M (2015) Fabrication and characterization of titania nanotube/cobalt sulfide supercapacitor electrode in various electrolytes. Chem Eng J 260:671–683
10. Jiang YZ, Li ZH, Li BB, Zhang JY, Niu CM (2016) Ni_3Si_2 nanowires grown in situ on Ni foam for high-performance supercapacitors. J Power Sources 320:13–19
11. Cui CY, Xu JT, Wang L, Guo D, Mao ML, Ma JM et al (2016) Growth of $NiCo_2O_4$@$MnMoO_4$ nanocolumn arrays with superior pseudocapacitor properties. ACS Appl Mater Interfaces 8:8568–8575
12. Jabeen N, Xia QY, Yang M, Xia H (2016) Unique core-shell nanorod arrays with polyaniline deposited into mesoporous $NiCo_2O_4$ support for high-performance supercapacitor electrodes. ACS Appl Mater Interfaces 8: 6093–6100
13. Cheng JB, Yan HL, Lu Y, Qiu KW, Hou XY, Xu JY et al (2015) Mesoporous $CuCo_2O_4$ nanograsses as multi-functional electrodes for supercapacitors and electro-catalysts. J Mater Chem A 3:9769–9776
14. Liu T, Chai H, Jia DZ, Su Y, Wang T, Zhou WY (2015) Rapid microwave-assisted synthesis of mesoporous $NiMoO_4$ nanorod/reduced graphene oxide composites for high-performance supercapacitors. Electrochim Acta 180:998–1006
15. Xia XF, Lei W, Hao QL, Wang WJ, Wang X (2013) One-step synthesis of $CoMoO_4$/graphene composites with enhanced electrochemical properties for supercapacitors. Electrochim Acta 99:253–261
16. Zhang Q, Deng YH, Hu ZH, Liu YF, Yao MM, Liu PP (2014) Seaurchin-like hierarchical $NiCo_2O_4$@$NiMoO_4$ core-shell nanomaterials for high performance supercapacitors. Phys Chem Chem Phys 16:23451–23460
17. An CH, Wang YJ, Huang YN, Xu YN, Xu CC, Jiao LF et al (2014) Novel three-dimensional $NiCo_2O_4$ hierarchitectures: solvothermal synthesis and electrochemical properties. CrystEngComm 16:385–392
18. Li SZ, Wen J, Chen T, Xiong LB, Wang JB, Fang GJ (2016) In situ synthesis of 3D CoS nanoflake/$Ni(OH)_2$ nanosheet nanocomposite structure as a candidate supercapacitor electrode. Nanotechnology 27:145401–145409
19. Zhang Y, Xu J, Zhang YJ, Hu XY (2016) 3D NiS dendritic arrays on nickel foam as binder-free electrodes for supercapacitors. J Mater Sci Mater Electron 27:8599–8605
20. Zhang Y, Xu J, Zheng YY, Hu XY, Shang YY, Zhang YJ (2016) Interconnected CuS nanowalls with rough surfaces grown on nickel foam as high-performance electrodes for supercapacitors. RSC Adv 6:59976–59983
21. Wang XH, Gao J, Wu XX, Wang XQ, Que RH, Wu KL (2016) A facile one-pot hydrothermal synthesis of Co_9S_8/Ni_3S_2 nanoflakes for supercapacitor application. RSC Adv 6:54142–54148
22. Niu LY, Wang YD, Ruan FP, Shen C, Shan S, Xu M et al (2016) In situ growth of $NiCo_2S_4$@$Ni_3V_2O_8$ on Ni foam as a binder-free electrode for asymmetric supercapacitors. J Mater Chem A 4:5669–5677
23. Tang JH, Ge YC, Shen JF, Ye MX (2016) Facile synthesis of $CuCo_2S_4$ as a novel electrode material for ultrahigh supercapacitor performance. Chem Commun 52:1509–1512
24. Hao L, Shen LF, Wang J, Xu YL, Zhang XG (2016) Hollow $NiCo_2S_4$ nanotube arrays grown on carbon textile as a self-supported electrode for asymmetric supercapacitors. RSC Adv 6:9950–9957
25. Cai DP, Wang DD, Wang CX, Liu B, Wang LL, Liu Y et al (2015) Construction of desirable $NiCo_2S_4$ nanotube arrays on nickel foam substrate for pseudocapacitors with enhanced performance. Electrochim Acta 151:35–41
26. Yan ML, Yao YD, Wen JQ, Long L, Kong ML, Zhang GG et al (2016) Construction of a hierarchical $NiCo_2S_4$@PPy core-shell heterostructure nanotube array on Ni foam for a high-performance asymmetric supercapacitor. ACS Appl Mater Interfaces 8:24525–24535
27. Liu XY, Shi SJ, Xiong QQ, Li L, Zhang YJ, Tang H et al (2013) Hierarchical $NiCo_2O_4$@$NiCo_2O_4$ core/shell nanoflake arrays as high-performance supercapacitor materials. ACS Appl Mater Interfaces 5:8790–8795
28. Yang YF, Cheng D, Chen SJ, Guan YL, Xiong J (2016) Construction of hierarchical $NiCo_2S_4$@$Ni(OH)_2$ core-shell hybrid nanosheet arrays on Ni foam for high-performance aqueous hybrid supercapacitors. Electrochim Acta 193:116–127
29. Li R, Wang SL, Huang ZC, Lu FX, He TB (2016) $NiCo_2S_4$@$Co(OH)_2$ core-shell nanotube arrays in situ grown on Ni foam for high performances asymmetric supercapacitors. J Power Sources 312:156–164
30. Huang L, Zhang W, Xiang JW, Xu HH, Li GL, Huang YH (2016) Hierarchical core-shell $NiCo_2O_4$@$NiMoO_4$ nanowires grown on carbon cloth as integrated electrode for high-performance supercapacitors. Sci Rep 6:31465–31472
31. Zhang YR, Yang YF, Mao LX, Cheng D, Zhan ZY, Xiong J (2016) Growth of three-dimensional hierarchical Co_3O_4@$NiMoO_4$ core-shell nanoflowers on Ni foam as electrode materials for hybrid supercapacitors. Mater Lett 182:298–301
32. Jiang G, Zhang MY, Li XQ, Gao H (2015) $NiMoO_4$@$Ni(OH)_2$ core/shell nanorods supported on Ni foam for high-performance supercapacitors. RSC Adv 5:69365–69370
33. Ma ZP, Shao GJ, Fan YQ, Wang GL, Song JJ, Shen DJ (2016) Construction of hierarchical α-MnO_2 nanowires@ultrathin δ-MnO_2 nanosheets core-shell nanostructure with excellent cycling stability for high-power asymmetric supercapacitor electrodes. ACS Appl Mater Interfaces 8:9050–9058
34. Wang XZ, Xiao YH, Su DC, Zhou LM, Wu SD, Han LF et al (2016) High-quality porous cobalt monoxide nanowires@ultrathin manganese dioxide sheets core-shell nanowire arrays on Ni foam for high-performance supercapacitor. Electrochim Acta 194:377–384
35. Cai DP, Wang DD, Lin B, Wang LL, Liu Y, Li H et al (2014) Three-dimensional Co_3O_4@$NiMoO_4$ core/shell nanowire arrays on Ni foam for electrochemical energy storage. ACS Appl Mater Interfaces 6:5050–5055
36. Xiao K, Xia L, Liu GX, Wang SQ, Ding LX, Wang HH (2015) Honeycomb-like $NiMoO_4$ ultrathin nanosheet arrays for high-performance electrochemical energy storage. J Mater Chem A 3:6128–6135
37. Kong W, Lu CC, Zhang W, Pu J, Wang ZH (2015) Homogeneous core-shell $NiCo_2S_4$ nanostructures supported on nickel foam for supercapacitors. J Mater Chem A 3:12452–12460
38. Hong W, Wang JQ, Gong PW, Sun JF, Niu LY, Yang ZG, Wang ZF, Yang SR (2014) Rational construction of three dimensional hybrid Co_3O_4@$NiMoO_4$ nanosheets array for energy storage application. J Power Sources 270:516–525
39. Pu J, Wang TT, Wang HY, Tong Y, Lu CC, Kong W, Wang ZH (2014) Direct growth of $NiCo_2S_4$ nanotube arrays on nickel foam as high-performance binder-free electrodes for supercapacitors. ChemPlusChem 79:577–583
40. Zhang ZQ, Bao FX, Zhang YN, Feng LK, Ji Y, Zhang HD et al (2015) Formation of hierarchical $CoMoO_4$@MnO_2 core-shell nanosheet arrays on nickel foam with markedly enhanced pseudocapacitive properties. J Power Sources 296:162–168
41. Zhang ZM, Wang Q, Zhao CJ, Min S, Qian XZ (2015) One-step hydrothermal synthesis of 3D petal-like Co_9S_8/RGO/Ni_3S_2 composite on nickel foam for high-performance supercapacitors. ACS Appl Mater Interfaces 7:4861–4868
42. Hu J, Li MC, Lv FC, Yang MY, Tao PP, Tang YG et al (2015) Heterogeneous $NiCo_2O_4$@polypyrrole core/sheath nanowire arrays on Ni foam for high performance supercapacitors. J Power Sources 294:120–127
43. Zhou XY, Chen GH, Tang JJ, Ren YP, Yang J (2015) One-dimensional $NiCo_2O_4$ nanowire arrays grown on nickel foam for high-performance lithium-ion batteries. J Power Sources 299:97–103
44. Ding R, Qi L, Wang HY (2013) An investigation of spinel $NiCo_2O_4$ as anode for Na-ion capacitors. Electrochim Acta 114:726–735
45. Patil AM, Lokhande AC, Chodankar NR, Kumbhar VS, Lokhande CD (2016) Engineered morphologies of β-NiS thin films via anionic exchange process and their supercapacitive performance. Mater Design 97:407–416
46. Ding R, Qi L, Jia MJ, Wang HY (2013) Facile and large-scale chemical synthesis of highly porous secondary submicron/micron-sized $NiCo_2O_4$ materials for high-performance aqueous hybrid AC-$NiCo_2O_4$ electrochemical capacitors. Electrochim Acta 107:494–502

47. Senthilkumar ST, Fu NQ, Liu Y, Wang Y, Zhou LM, Huang HT (2016) Flexible fiber hybrid supercapacitor with $NiCo_2O_4$ nanograss@carbon fiber and bio-waste derived high surface area porous carbon. Electrochim Acta 211:411–419
48. Kuang M, Wen ZQ, Guo XL, Zhang SM, Zhang YX (2014) Engineering firecracker-like beta-manganese dioxides@spinel nickel cobaltates nanostructures for high-performance supercapacitors. J Power Sources 270:426–433
49. Kuang M, Zhang YX, Li TT, Li KF, Zhang SM, Li G et al (2015) Tunable synthesis of hierarchical $NiCo_2O_4$ nanosheets-decorated Cu/CuOx nanowires architectures for asymmetric electrochemical capacitors. J Power Sources 283:270–278
50. Zeng ZF, Wang DZ, Zhu JL, Xiao FQ, Li YD, Zhu XH (2016) $NiCo_2S_4$ nanoparticles//activated balsam pear pulp for asymmetric hybrid capacitors. CrystEngComm 18:2363–2374